Available online at www.sciencedirect.com

ScienceDirect

Ceramics International 40 (2014) 217–225

CERAMICS INTERNATIONAL

www.elsevier.com/locate/ceramint

Properties of heavily W-doped TiO_2 films deposited on Al_2O_3-deposited glass by simultaneous rf and dc magnetron sputtering

Su-Shia Lin*

Department of Applied Materials and Optoelectronic Engineering, National Chi Nan University, Puli, Nantou Hsien 54561, Taiwan, ROC

Received 2 April 2013; received in revised form 27 May 2013; accepted 31 May 2013
Available online 6 June 2013

Abstract

TiO_2 films were heavily doped with W (TiO_2:W) by simultaneous rf magnetron sputtering of TiO_2, and dc magnetron sputtering of W. The advantage of this method is that the W content could be changed in a wide range. The coexistence of TiO_2, WO_3 and $TiWO_5$ in the TiO_2:W film was detected by XPS analysis. Besides, tungsten in TiO_2:W film on the bare glass may form mixed valence of W^{0+} and W^{6+}. Electrical conductivity was primarily due to the contribution of oxygen vacancies and W donors ($W_{Ti}^{\bullet\bullet}$). When the film thickness increased, the TiO_2:W film showed higher carrier concentration and higher mobility. Furthermore, the resistivity and the transmission decreased obviously with film thickness. On comparing with the TiO_2:W film deposited on the bare glass, the TiO_2:W film on the Al_2O_3-deposited glass exhibited lower surface roughness, lower resistivity, higher optical energy gap, higher optical transmission, and lower stress-optical coefficient.

Keywords: Film; Sputtering; Resistivity; Optical energy gap

1. Introduction

Titanium dioxide is a material widely used in the ceramic, cosmetic, coating, automobile and pigment industries. Nowadays it has been one of the most extensively studied oxides because of its remarkable optical and electrical properties [1,2]. Compared with other semiconductors, the great advantages of TiO_2 lie in the fact that it possesses appropriate flat band potential and high chemical stability. To date, TiO_2 is still the leading photocatalyst because it can mineralize a large range of organic pollutants [3,4]. However, due to its large band gap energy (typically < 380 nm), TiO_2 can only absorb ultraviolet light rather than visible light that occupies the great part of solar light. Furthermore, the overall quantum yield rate can be influenced by the low rate of electron transfer to dissolved oxygen and a high rate of recombination between electron–hole pairs [5]. Thus, much effort has been made to decrease the band gap energy of TiO_2 by doping TiO_2 with main group elements including carbon, nitrogen and sulfur [6–8], transition metal elements such as W^{6+}, Fe^{3+}, Zr^{4+}, V^{5+} and Mo^{6+} [9–12]. Among transition metal elements, W^{6+} ion can substantially reduce the recombination process between dopant cation and TiO_2 matrixes. It seems to be an interesting dopant to extend the absorption threshold toward the visible range. Besides, Jo et al. [13] studied WO_3 doped TiO_2 thick film deposited by screen printing, and reported an electrical interaction between WO_3 and TiO_2 for high temperature gas sensors.

Different methods, such as chemical, physical deposition processes, and ion implantation can be selectively employed to dope TiO_2 films [14]. Among the physical vapor deposition (PVD) techniques, magnetron sputtering has the advantage of being scalable to large-area industrial processes and has shown to be an efficient way to prepare and dope high-quality TiO_2 films [15]. Because doped films generally can be caused to have very stable optical and electrical properties [16]. Furthermore, studies of the conduction mechanism in heavily W-doped TiO_2 (TiO_2:W) thin films prepared by magnetron sputtering have not been reported. In this work, the TiO_2 films

*Tel.: +886 49 2910960x4771; fax: +886 49 2912238.
E-mail address: sushia@ncnu.edu.tw

0272-8842/$ - see front matter © 2013 Elsevier Ltd and Techna Group S.r.l. All rights reserved.
http://dx.doi.org/10.1016/j.ceramint.2013.05.126

were heavily doped with W (TiO_2:W) by simultaneous rf magnetron sputtering of TiO_2, and dc magnetron sputtering of W. The advantage of this kind of deposited method is that the W content could be changed in a wide range.

Aluminum oxide is a very promising layer material because of its interesting optical properties and low cost [17]. The formation of fibered morphology of Al_2O_3 film was dominated by low Ar pressure, and was good for optical properties [18]. Besides, the glass has been widely used in optical devices and has many important applications. Thus, the Al_2O_3 film exhibiting fibered morphology was deposited on the glass and acted as the substrate in this study. The characteristics of films are affected by the preparation conditions such as working pressure, substrate temperature, types of substrates, and the thickness of the films [19,20]. The influence of types of substrates (bare glass and Al_2O_3-deposited glass) and film thickness on optical and electrical properties of TiO_2:W films was investigated.

2. Experimental procedures

The Al_2O_3-deposited glass and TiO_2:W films were prepared by magnetron sputtering. The targets used in this study were sintered stoichiometric Al_2O_3 (99.99% purity, 5 cm diameter, 5 mm thickness, Target Materials Inc., USA), sintered stoichiometric TiO_2 (99.99% purity, 5 cm diameter, 5 mm thickness, Target Materials Inc., USA) and metallic W (99.95% purity, 5 cm diameter, 5 mm thickness, Target Materials Inc., USA).

The dimension of the glass substrates (Corning 1737) was 24 mm × 24 mm × 1.1 mm. Before deposition, the substrates were ultrasonically cleaned in alcohol, rinsed in deionized water and dried in nitrogen. For the deposition of the films, the sputtering was performed in a pure Ar with a target-to-substrate distance of 15 cm. The substrate was not heated and no external bias voltage was applied to the substrate. The rotating speed of the substrate was 20 rpm.

A turbo-molecular pump backed by a rotary pump, was used to achieve a base pressure of 1.3×10^{-4} Pa. At a working pressure of 0.29 Pa, an rf power (13.56 MHz, RGN-1302, ULVAC, Japan) of 200 W was supplied to the Al_2O_3 target and the Al_2O_3 film was deposited to a thickness of 100 nm. On the Al_2O_3-deposited glass, the TiO_2:W film with a thickness of 20–300 nm was deposited at a working pressure of 1.5 Pa. An rf power (13.56 MHz, RGN-1302, ULVAC, Japan) of 50 W was supplied to the TiO_2 target, and a dc power (DCS0052B, ULVAC, Japan) of 6 W was applied to the W target.

Film thickness was measured using a surface profiler (Alpha-Step 500, TENCOR, Santa Clara, CA). Surface morphologies and surface roughness were examined by atomic force microscopy (AFM; Agilent 5500, Santa Clara, CA). Elemental compositions were investigated by X-ray photoemission spectroscopy (XPS; PHI 5000 VersaProbe, Japan). The optical transmission spectra of films in the ultraviolet–visible–near infrared (UV–VIS–NIR) region were obtained using a spectrophotometer (HP 8452A diode array spectrophotometer, Hewlett Packard, Palo Alto, CA). The resistivity, mobility, and carrier concentration were measured by a Hall Effect Measurement System (HMS-2000, ECOPIA, USA). Linear refractive indices of samples were recorded using a spectrometer (MP100-ST, Fremont, CA). Young's modulus was measured by the Nano Indenter XP System (MTS Systems Corporation, MN, USA).

Fig. 1 shows the Moiré deflectometry experimental set-up that is used to measure the nonlinear refractive indices of TiO_2:W films on the bare glass and the Al_2O_3-deposited glass. Lens L_1 focused a 5-mW He–Ne laser beam (wavelength of 632.8 nm), which was re-collimated by lens L_2. The focal lengths of lenses L_1, L_2 and L_3 were all –250 mm. Two similar Ranchi gratings, G_1 and G_2 with a pitch of 0.1 mm were used to construct the Moiré fringe patterns. The distance between the planes of G_1 and G_2 was set to 64 mm, which is one of the Talbot distances of the used gratings. The Talbot distances satisfy $z_t = tp^2/\lambda$ where p is the periodicity of the grating; λ is the wavelength of light, and t is an integer. In this work, the Moiré fringes were clearly formed at a Talbot distance of $z_{t=4} \approx 64$ mm. The Moiré fringe patterns were projected onto a computerized CCD camera by lens L_3, which was placed at the back of the second grating.

3. Results and discussion

3.1. The effect of Al_2O_3-deposited glass substrate

Fig. 2 shows the morphologies of (a) Al_2O_3-deposited glass, (b) TiO_2:W film on the Al_2O_3-deposited glass (sample A) and (c) TiO_2:W film on the bare glass (sample B). In Fig. 2a, the fibered morphology is a consequence of the nucleation of grains that grow geometrically and impinge laterally. It is a result of a competition during deposition between the rate of arrival of new Al_2O_3 species on the surface and the concurrent redistribution over the surface by diffusion. Hence, the fibered morphology may be due to the nonequilibrium growth [18]. The advantages of Al_2O_3 film with fibered morphology were described in a previous paper [18]. According to Fig. 2b and c, sample A and sample B were composed of irregular grains with island structures, but sample A exhibited lower roughness. The roughness values were very close to the morphologies of growing films [21]. Generally, the surface roughness could affect the carrier mobility [22].

The bonding conditions of oxygen on the surfaces of TiO_2:W films were investigated by XPS spectra. Fig. 3 shows Ti 2p photoelectron peaks in the XPS spectra of (a) TiO_2:W film on the Al_2O_3-deposited glass (sample A) and (b) TiO_2:W film on

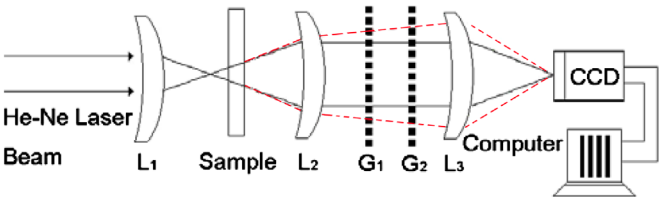

Fig. 1. The experimental set-up for measuring nonlinear refractive index by the Moiré deflectometry technique.

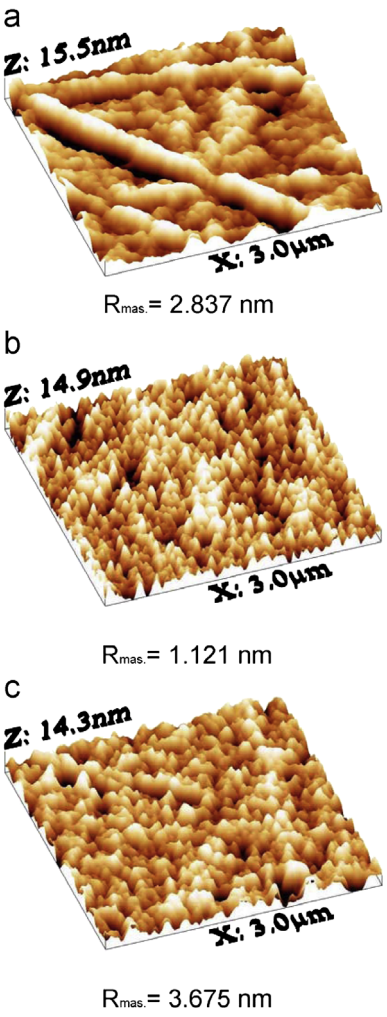

Fig. 2. The morphologies of (a) Al_2O_3-deposited glass, (b) TiO_2:W film on the Al_2O_3-deposited glass (sample A) and (c) TiO_2:W film on the bare glass (sample B).

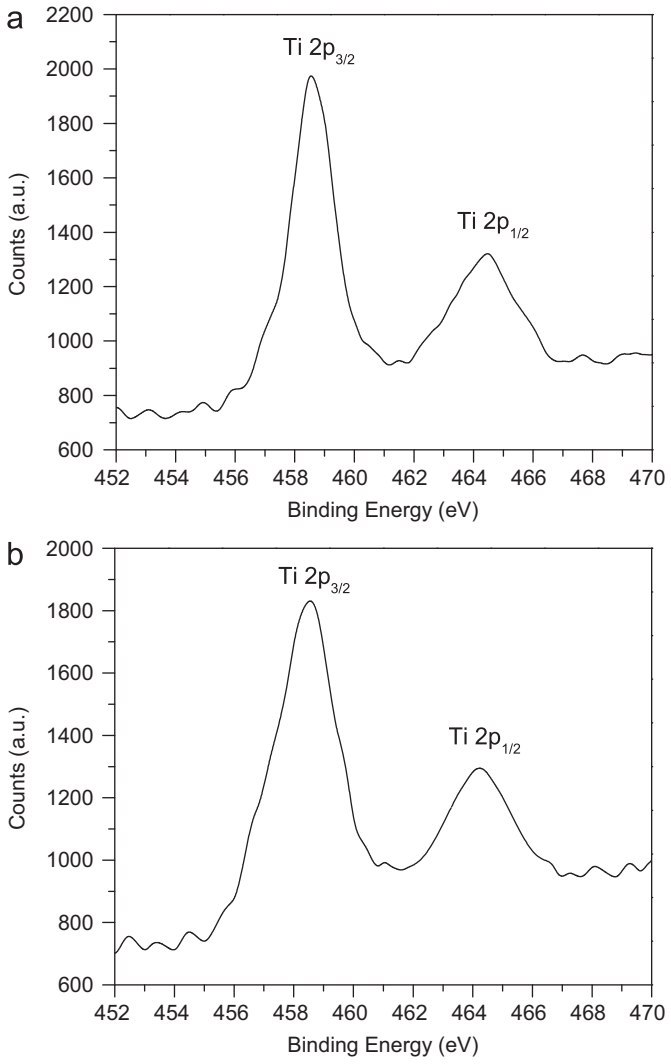

Fig. 3. Ti 2p photoelectron peaks in the XPS spectra of (a) TiO_2:W film on the Al_2O_3-deposited glass (sample A) and (b) TiO_2:W film on the bare glass (sample B).

the bare glass (sample B). The Ti 2p spectra consists of Ti $2p_{3/2}$ and Ti $2p_{1/2}$ peaks. In Fig. 3a and b, the binding energy corresponding to the Ti $2p_{3/2}$ state (458.5 ± 0.02 eV) in the measured samples is shifted by 5 eV as compared with metallic titanium (453.5 eV). The binding energy shift of this value indicates that the films contain titanium at the highest oxidation state Ti^{4+} [23]. The highest and the lowest energy components have been assigned to Ti^{4+} and Ti^0, respectively, while the intermediate component has the energy shift relative to TiO_2 that falls in between that of Ti^{3+} and Ti^{2+} [24]. According to Fig. 3a and b, no energy shift relative to TiO_2 could be observed. It suggested that the contribution of oxidation states of Ti was probably only due to Ti^{4+} for sample A and sample B.

Fig. 4 shows W 4f photoelectron peaks in the XPS spectra of (a) TiO_2:W film on the Al_2O_3-deposited glass (sample A) and (b) TiO_2:W film on the bare glass (sample B). In Fig. 4a, peaks of W $4f_{7/2}$ at 35.5 ± 0.01 eV and W $4f_{5/2}$ at 37.4 ± 0.03 eV, which indicated that the film contained tungsten at the highest oxidation state W^{6+} [25]. In Fig. 4b, peaks of W $4f_{7/2}$ at 35.5 ± 0.01 eV and W $4f_{5/2}$ at 37.6 ± 0.01 eV, which were attributed to W oxides [26]. Meanwhile, peaks of W $4f_{7/2}$ at 31.2 ± 0.09 eV and W $4f_{5/2}$ at 33.1 ± 0.08 eV, which were attributed to W metal [26]. It suggested that tungsten in sample B may form mixed valence of W^{0+} and W^{6+}. By comparing Fig. 4a with b, metallic tungsten (W^{0+}) presented preferentially and as interstitial atoms in the lattice of TiO_2:W film on the bare glass.

Fig. 5 shows O 1s photoelectron peaks in the XPS spectra of (a) TiO_2:W film on the Al_2O_3-deposited glass (sample A) and (b) TiO_2:W film on the bare glass (sample B). In Fig. 5a, the O 1s peak was composed of three peaks (O_I, O_{II} and O_{III}). The peak (O_I) at 531.2 ± 0.01 eV may be due to oxygen in TiO_2 [27]. The peak (O_{II}) at 530.2 ± 0.02 eV could be attributed to oxygen in WO_3 [25]. The peak (O_{III}) at 529.6 ± 0.01 eV was speculated and probably due to oxygen in $TiWO_5$. In Fig. 5b, the O 1s peak was composed of three peaks (O_I, O_{II} and O_{III}). The peak (O_I) at 531.2 ± 0.01 eV may be due to oxygen in TiO_2, whereas the peak (O_{II}) at 530.2 ± 0.01 eV was probably due to oxygen in WO_3. The peak (O_{III}) at 529.6 ± 0.01 eV was speculated and probably due to oxygen in $TiWO_5$.

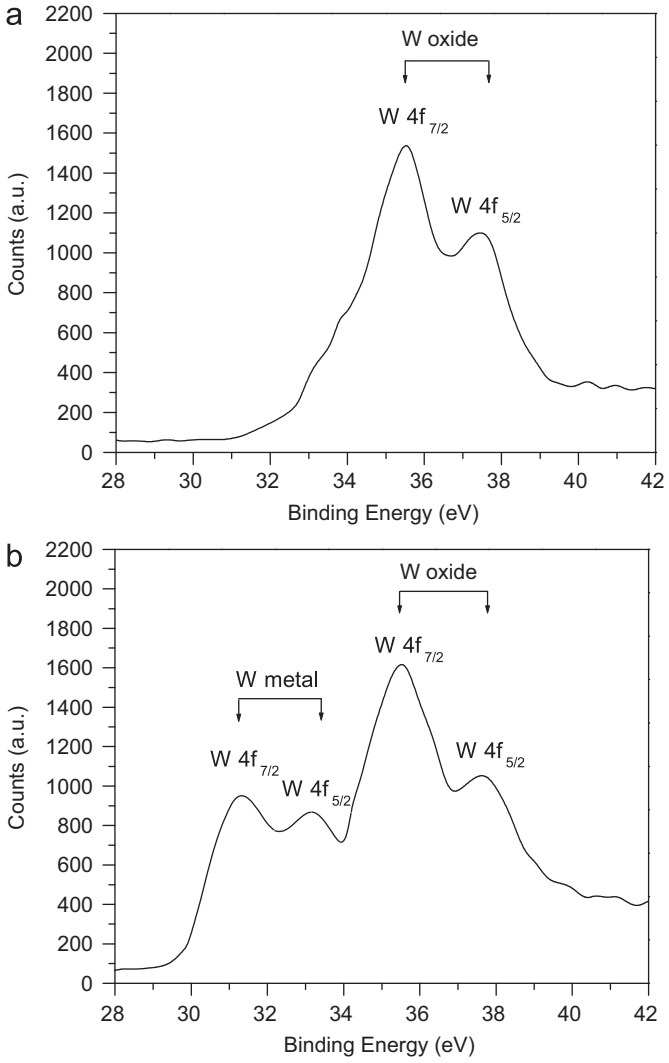

Fig. 4. W 4f photoelectron peaks in the XPS spectra of (a) TiO_2:W film on the Al_2O_3-deposited glass (sample A) and (b) TiO_2:W film on the bare glass (sample B).

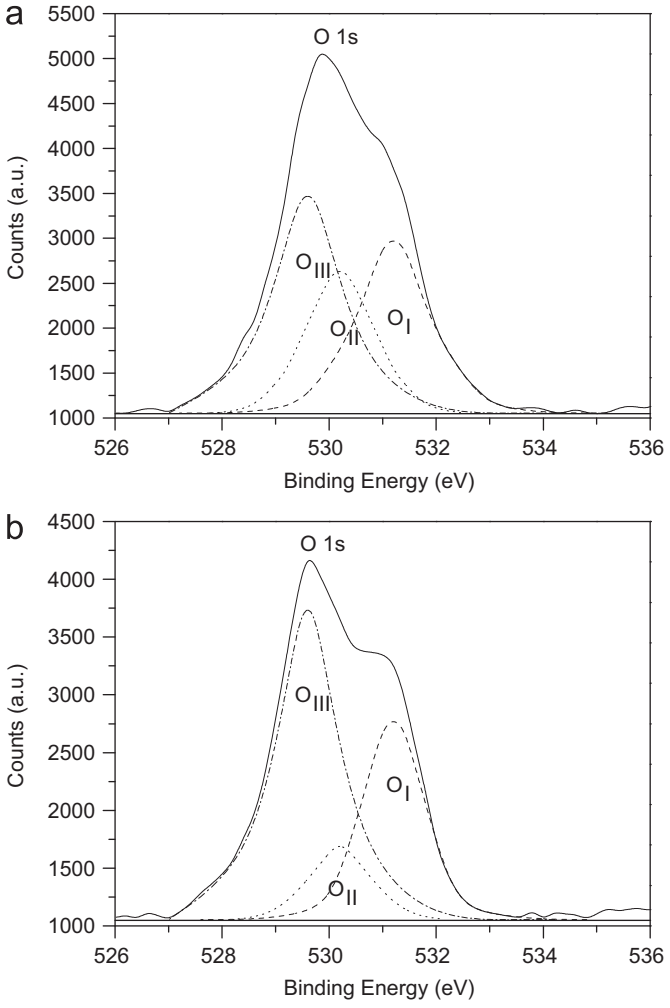

Fig. 5. O 1s photoelectron peaks in the XPS spectra of (a) TiO_2:W film on the Al_2O_3-deposited glass (sample A) and (b) TiO_2:W film on the bare glass (sample B).

We defined the relative strength of a peak as the ratio of its area to the total area of O_I, O_{II} and O_{III} peaks. According to Fig. 5a and b, the relative strength of O_{II} was relatively low, especially for sample B. It suggested that Ti atoms in TiO_2 crystalline were not substituted favorably by W atoms for the TiO_2:W films, especially on the bare glass.

By XPS measurement, Ti, W and O contents of sample A were 20.6 at%, 13.4 at% and 66 at%, respectively. Similar results were obtained for sample B. The O/(Ti+W) atomic ratio was below 2, suggesting that the deposited films became nonstoichiometric. It also suggested that the formation of oxygen vacancies in the TiO_2:W films.

Results of Hall measurements (Table 1) revealed that TiO_2:W films are of electrical properties. Sample A showed lower resistivity, higher mobility and carrier concentration. Igasaki and Saito [28] reported that an increase in conduction electrons could be attributed to the increase in donors and/or oxygen vacancies in which incorporation of donors takes place. According to the preceding discussion (Figs. 3–5), the conduction electrons of TiO_2:W films may be originated from the oxygen vacancies ($V_o^{\bullet\bullet}$) and W donors ($W_{Ti}^{\bullet\bullet}$) as shown.

$$WO_3 \xrightarrow{TiO_2} W_{Ti}^{\cdot\cdot} + 3O_o + V_o^{\cdot\cdot} + 4e' \quad (1)$$

Besides, the resistivity ρ is proportional to the reciprocal of the product of carrier concentration N and mobility μ as the following equation [29]:

$$\rho = \frac{1}{Ne\mu} \quad (2)$$

In Table 1, the lower resistivity of TiO_2:W film was probably caused by the product of carrier concentration N and mobility μ being relatively high. For sample A, Ti atoms in TiO_2 crystalline were substituted favorably by W atoms, which caused higher carrier concentration. Furthermore, sample A exhibited lower roughness, which corresponded to higher mobility.

A change of the linear refractive index caused by stress is called the photoelastic effect [30]. The linear refractive index is specified by the indicatrix, which is an ellipsoid whose coefficients are the components of the relative dielectric

Table 1
Resistivity, mobility, carrier concentration, linear refractive index and Young's modulus of TiO_2:W films deposited on the different substrates.

Sample	A	B
Film	TiO_2:W	TiO_2:W
Film thickness (nm)	300	300
Substrate	Al_2O_3-deposited glass	Bare glass
Resistivity ρ (Ω-cm)	1.979	7.202
Mobility μ (cm^2/V-s)	103.86	71.13
Carrier concentration N (cm^{-3})	3.04×10^{16}	1.22×10^{16}
Linear refractive index n_0	2.305	2.187
Young's modulus (GPa)	54.7	65.6

impermeability tensor B_{ij} at optical frequencies:

$$B_{ij}x_ix_j = 1 \quad (3)$$

The small change of the linear refractive index produced by stress is a small change in the shape, size and orientation of the indicatrix. This change is specified by the small changes in the coefficients B_{ij}.

If terms of higher-order than the first in the field of stresses are neglected, then the changes ΔB_{ij} in the coefficients are

$$\Delta B_{ij} = \varphi_{ijkl}\sigma_{kl} \quad \text{or} \quad \Delta B_{ij} = p_{ijrs}\varepsilon_{rs} \quad (4)$$

where φ_{ijkl} and p_{ijrs} are called the piezo-optical and strain-optical coefficients, which typically have the orders of magnitude of 10^{-12} Pa^{-1} and 10^{-1} Pa^{-1}, respectively.

Based on the relation, $B = 1/n_0^2$, the change of linear refractive index for an isotropic film material is assumed to be [30,31]

$$\left(\frac{\partial n_0}{\partial \sigma}\right)_T = -\frac{1}{2}n_0^3\varphi \quad (5)$$

$$\boldsymbol{\sigma} = E\varepsilon \quad (6)$$

where σ is the stress, E is the Young's modulus, and ε is strain. Young's modulus is related to the bonding strength between the atoms in material, and is proportional to stress [32]. Consequently, a change in the linear refractive index due to film stress may affect the optical performance of an optical thin film, as shown in Eq. (5).

By consulting similar studies of films for nanoindentation tests [33–36], the measured indentation moduli of the films could be influenced by the substrate even at indentation depths less than 2% of the film thickness. As the indenter goes deeper into the film, the effects caused by indenter oscillation become negligible and the substrate effect dominates the indentation process. For the measurement of elastic modulus of the film, the result will be greatly affected by the substrate even if the indentation depth is very small because the elastic deformation is not confined to the film itself; rather, it is a long-range effect that extends into the substrate [34]. According to Table 1, sample A showed higher linear refractive index and lower Young's modulus. The reason was probably due to Al_2O_3-deposited glass being able to absorb more applied strain [37].

The value of $\Delta n_0/\Delta E$ is equal to the value of $\Delta n_0/\Delta\sigma$. Furthermore, the value of $\Delta n_0/\Delta\sigma$ is reportedly similar to the stress-optical coefficient [38]. The stress-optical coefficient, $(\partial n_0/\partial\sigma)_T$ of sample A was lower than that of sample B, and was calculated to be in the range of -5.2×10^{-12} to -13.7×10^{-12} Pa^{-1}.

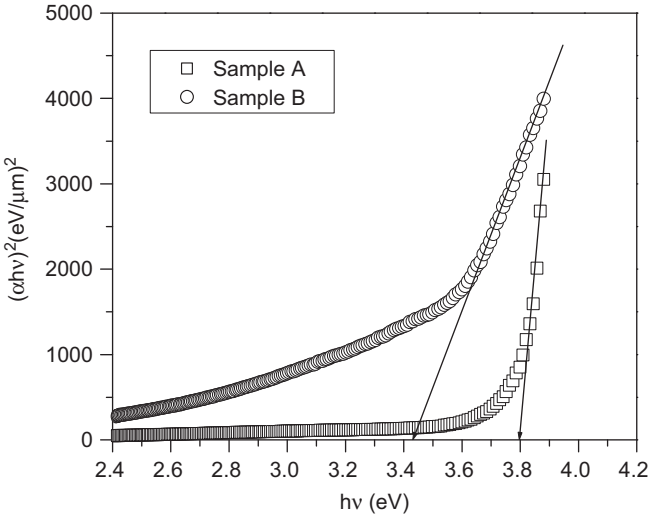

Fig. 6. Plots of $(\alpha h\nu)^2$ versus $h\nu$ for TiO_2:W films deposited on the Al_2O_3-deposited glass (sample A) and the bare glass (sample B).

The optical energy gap E_g could be obtained from the intercept of $(\alpha h\nu)^2$ versus $h\nu$ for direct allowed transitions [39]. Better linearity was observed for $(\alpha h\nu)^2$ versus $h\nu$ [39,40] as shown in Fig. 6. Fig. 6 shows the plots of $(\alpha h\nu)^2$ versus $h\nu$ for TiO_2:W films deposited on the Al_2O_3-deposited glass (sample A) and the bare glass (sample B). The values of E_g were 3.8 eV and 3.43 eV for sample A and sample B, respectively. The change of optical energy gap for sample B has been interpreted as a Moss–Burstein shift, where the change is the result of the decrease in the free carrier concentration, and the corresponding downward shift of the Fermi level to below the band edge [41,42]. The carrier concentration of TiO_2:W film (Table 1) was closely related to optical energy gap (Fig. 6).

Fig. 7 shows the transmission in the UV–VIS–NIR region of TiO_2:W films deposited on the Al_2O_3-deposited glass (sample A) and the bare glass (sample B). According to Figs. 6 and 7, sample A had higher optical energy gap and exhibited higher transmission. It was also probably due to the relatively low surface roughness, which could result in less light scattering [43]. The results indicated that the Al_2O_3-deposited glass

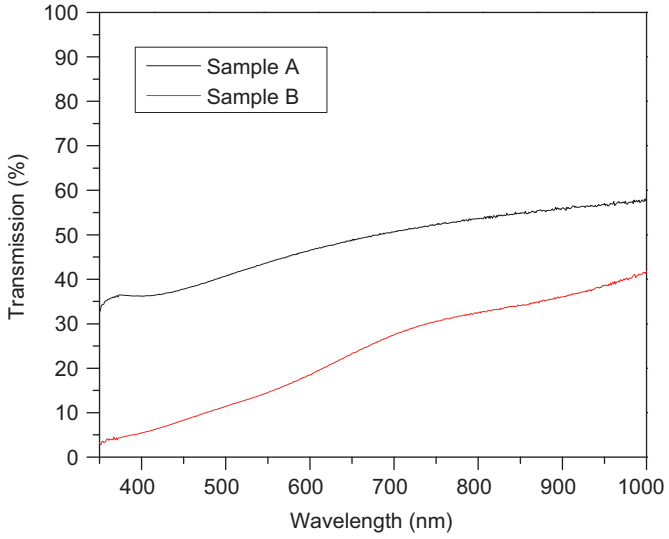

Fig. 7. The transmission in the UV–VIS–NIR region of TiO_2:W films deposited on the Al_2O_3-deposited glass (sample A) and the bare glass (sample B).

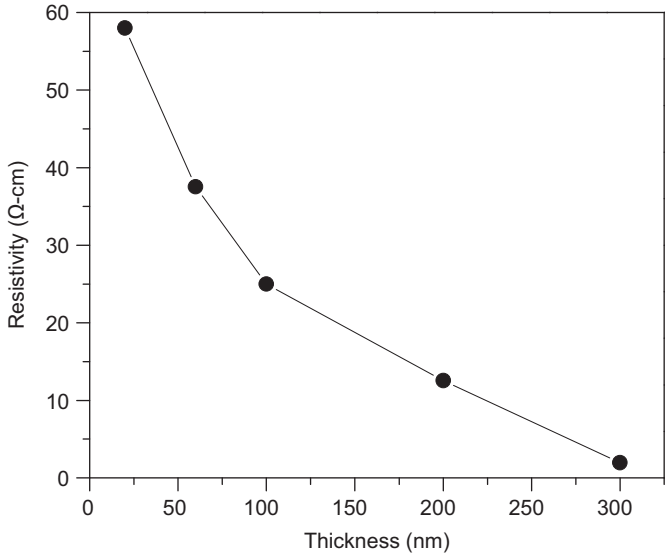

Fig. 8. The resistivity of sample A with different thicknesses.

substrate affected the optical transmission of TiO_2:W film significantly.

3.2. The effect of film thickness

Fig. 8 shows the resistivity of sample A with different thicknesses. The resistivity decreased with the film thickness. Chiou et al. [44] reported that the resistivity of thick film and thin film could be expressed by Eqs. (7) and (8), respectively.

$$\frac{\rho_f}{\rho_o} = 1 + \frac{3}{8K} \quad (K \gg 1) \tag{7}$$

$$\frac{\rho_f}{\rho_o} = \frac{4}{3K\ln\frac{1}{K}} \quad (K \ll 1) \tag{8}$$

Here ρ_f is the resistivity of thin film, ρ_o is the resistivity of bulk, and K is the reduced thickness. (K=the film thickness/the mean free path of the charge carrier in the bulk material). From Eqs. (7) and (8), it can be seen that the film thickness affects the resistivity of thin film more than thick film. In addition, the resistivity decreased with the increase of film thickness. The resistivity of TiO_2:W films in this study had a similar behavior.

Fig. 9 shows the mobility and carrier concentration of sample A with different thicknesses. The mobility and carrier concentration increased with the increase of film thickness. On comparing Fig. 8 with Fig. 9, the TiO_2:W film with 300 nm thickness showed the lowest resistivity, which resulted from the highest product of carrier concentration and mobility.

Fig. 10 shows the transmission in the UV–VIS–NIR region of sample A with different thicknesses. The transmission in the UV–VIS–NIR region increased obviously with the decrease in film thickness.

Nonlinear refractive indices of materials are of great interest because of potential applications in designing optical devices and laser technology [45–48]. The refractive index, n, which

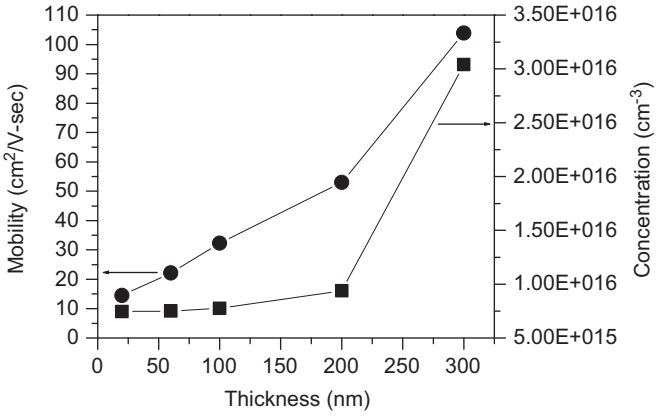

Fig. 9. The mobility and carrier concentration of sample A with different thicknesses.

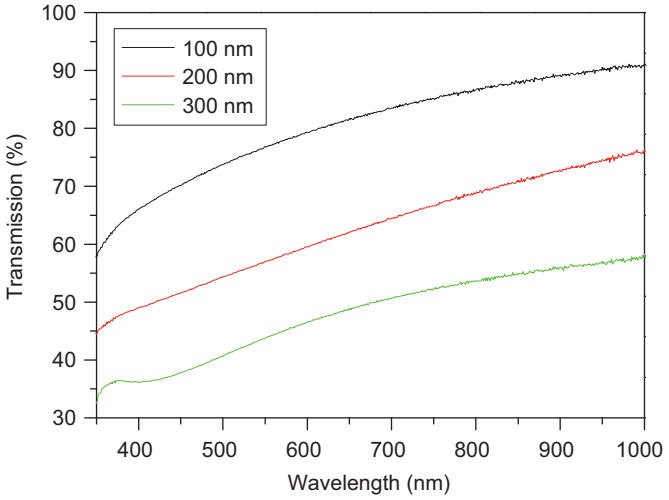

Fig. 10. The transmission in the UV–VIS–NIR region of sample A with different thicknesses.

depends on the radiation intensity, may be expressed in terms of the nonlinear refractive index n_2 ($cm^2\ W^{-1}$):

$$n(r,z) = n_o + n_2 I(r,z) = n_o + \Delta n(r,z) \tag{9}$$

where n_o is the linear refractive index, $I(r,z)$ is the irradiance of the laser beam within the sample, and $\Delta n(r,z)$ is the light-induced change in refractive index.

Based on the assumption that a Gaussian beam is traveling in the $+z$ direction, the beam irradiance can be written as

$$I(r,z) = I_0 \frac{\omega_0^2}{\omega^2(z)}\left[1-\frac{2r^2}{\omega^2(z)}\right] \tag{10}$$

where r is the radial radius of the imaginary sphere; ω_0 is the spot size of the beam at the focus; $\omega(z)=\omega_0(1+z^2/z_0^2)^{1/2}$ is the beam radius at a distance z from the position of the waist; $z_0 = \pi\omega_0^2/\lambda$ is the diffraction length of the Gaussian beam, and λ is the wavelength. The irradiance of the beam at the focus is denoted by I_0 and in terms of the input laser power, p_{in}, which equals $2p_{in}/\pi\omega_0^2$. Therefore, for a Gaussian laser beam, the radial dependence of the irradiance gives rise to a radially-dependent parabolic refractive index change near the beam axis:

$$\Delta n(r,z) = n_2 I_0 \frac{\omega_0^2}{\omega^2(z)}\left[1-\frac{2r^2}{\omega^2(z)}\right] \tag{11}$$

Moiré deflectometry is a sensitive technique for measuring changes in the refractive indices of materials. The sensitivity of this technique is determined by the minimum measurable-angle of rotation (α_{min}). Fig. 11 shows the Moiré fringe rotation angle versus z for sample A. The tested sample was placed at various distances from the focal point of lens L_1. The minimum angle of rotation was obtained from the figure. The same experiment was performed using only an Al_2O_3-deposited glass substrate to check the contribution of the substrate to the nonlinear refraction measurement. No observed fringe rotation or change in fringe size was found.

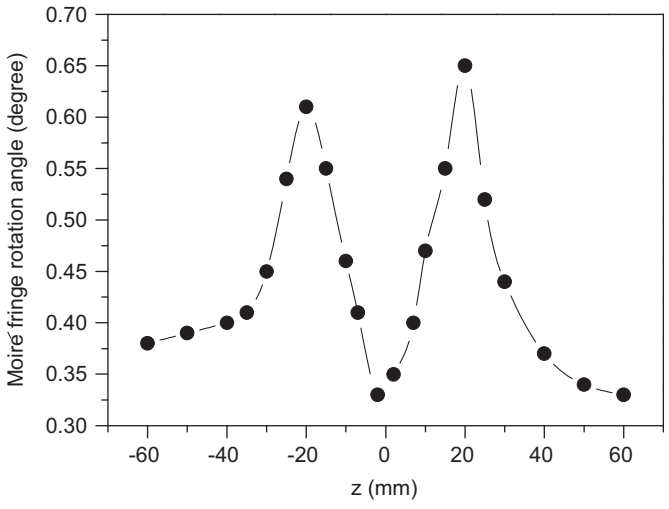

Fig. 11. The Moiré fringe rotation angle versus z for sample A.

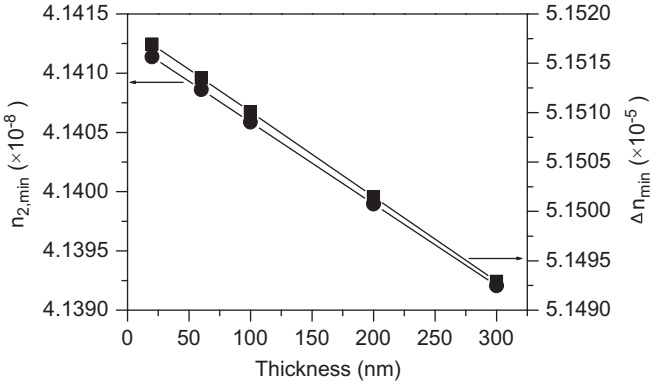

Fig. 12. Minimum nonlinear refractive indices and the change in the minimum refractive indices of sample A with different thicknesses.

For the thin nonlinear medium of thickness d, the lowest nonlinear refractive index can be written as

$$n_{2,min} = \frac{\theta f_2^2}{2z_t}\frac{\pi\omega_0^4}{2dp_{in}z_0^2}\alpha_{min} \tag{12}$$

and the change in the minimum refractive index is

$$\Delta n_{min} = \frac{\theta f_2^2\omega_0^2}{z_t}\frac{}{dz_0^2}\alpha_{min} \tag{13}$$

Fig. 12 shows the minimum nonlinear refractive indices and the change in the minimum refractive indices of sample A with different thicknesses. The nonlinear refractive index was measured to be of the order of $10^{-8}\ cm^2\ W^{-1}$ and the change in refractive index was of the order of 10^{-5}.

4. Conclusions

In this study, electrical conductivity was primarily due to the contribution of oxygen vacancies and W donors ($W_{Ti}^{\cdot\cdot}$). For the TiO_2:W film on the Al_2O_3-deposited glass, Ti atoms in TiO_2 crystalline were substituted favorably by W atoms, which caused the higher carrier concentration. However, metallic tungsten (W^{0+}) presented preferentially and as interstitial atoms in the lattice of TiO_2:W film on the bare glass. The TiO_2:W film with lower surface roughness corresponded to higher mobility, higher optical energy gap and higher optical transmission. The nonlinear refractive indices of TiO_2:W films on the Al_2O_3-deposited glass were measured to be of the order of $10^{-8}\ cm^2\ W^{-1}$. Furthermore, the resistivity and the transmission decreased obviously with film thickness. This suggested that the application of thicker TiO_2:W film was limited.

Acknowledgements

The author would like to thank the National Science Council of the Republic of China, Taiwan, for financially supporting this research under Contract no. NSC-99–2221-E-260-017.

References

[1] N.S.P. Bhuvanesh, J. Gopalakrishnan, Solid-state chemistry of early transition-metal oxides containing d^0 and d^1 cations, Journal of Materials Chemistry 7 (1997) 2297–2306.

[2] H. Poelman, D. Poelman, D. Depla, H. Tomaszewski, L. Fiermans, R. De Gryse, Electronic and optical characterization of TiO_2 films deposited from ceramic targets, Surface Science 482–485 (2001) 940–945.

[3] Z. Ding, G.Q. Lu, P.F. Greenfield, Role of the crystallite phase of TiO_2 in heterogeneous photocatalysis for phenol oxidation in water, Journal of Physical Chemistry B 104 (2000) 4815–4820.

[4] H. Einaga, S. Futamura, T. Ibusuki, Heterogeneous photocatalytic oxidation of benzene, toluene, cyclohexene and cyclohexane in humidified air: comparison of decomposition behavior on photoirradiated TiO_2 catalyst, Applied Catalysis B: Environmental 38 (2002) 215–225.

[5] X.Z. Li, F.B. Li, Study of Au/Au^{3+}-TiO_2 photocatalysts toward visible photooxidation for water and wastewater treatment, Environmental Science and Technology 35 (2001) 2381–2387.

[6] A.W. Morawski, M. Janus, B. Tryba, M. Inagaki, K. Kalucki, TiO_2-anatase modified by carbon as the photocatalyst under visible light, Comptes Rendus Chimie 9 (2006) 800–805.

[7] R. Asahi, T. Morikawa, T. Ohwaki, K. Aoki, Y. Taga, Visible-light photocatalysis in nitrogen-doped titanium oxides, Science 293 (2001) 269–271.

[8] T. Ohno, N. Murakami, T. Tsubota, H. Nishimura, Development of metal cation compound-loaded s-doped TiO_2 photocatalysts having a rutile phase under visible light, Applied Catalysis A 349 (2008) 70–75.

[9] Y.F. Shen, T.Y. Xiong, T.F. Li, K. Yang, Tungsten and nitrogen co-doped TiO_2 nanopowders with strong visible light response, Applied Catalysis B 83 (2008) 177–185.

[10] W.Y. Teoh, R. Amal, L. Mädler, S.E. Pratsinis, Flame sprayed visible light-active Fe–TiO_2 for photomineralisation of oxalic acid, Catalysis Today 120 (2007) 203–213.

[11] G.H. Tian, K. Pan, H.G. Fu, L.Q. Jing, W. Zhou, Enhanced photocatalytic activity of S-doped TiO_2–ZrO_2 nanoparticles under visible-light irradiation, Journal of Hazardous Materials 166 (2009) 939–944.

[12] A. Kubacka, G. Colón, M. Fernández-García, Cationic (V, Mo, Nb, W) doping of TiO_2-anatase: a real alternative for visible light-driven photocatalysts, Catalysis Today 143 (2009) 286–292.

[13] S.E. Jo, B.G. Kang, S. Heo, S. Song, Y.J. Kim, Gas sensing properties of WO_3 doped rutile thick film at high operating temperature, Current Applied Physics 9 (2009) e235–e238.

[14] M. Ni, M. Leung, D. Leung, K. Sumathy, A review and recent developments in photocatalytic water-splitting using TiO2 for hydrogen production, Renewable and Sustainable Energy Reviews 11 (2007) 401–425.

[15] G. Abadias, A.S. Gago, N. Alonso-Vante, Structural and photoelectrochemical properties of $Ti_{1-x}W_xO_2$ thin films deposited by magnetron sputtering, Surface and Coatings Technology 205 (2011) S265–S270.

[16] S.S. Lin, J.L. Huang, D.F. Lii, Effect of substrate temperature on the properties of Ti-doped ZnO films by simultaneous rf and dc magnetron sputtering, Materials Chemistry and Physics 90 (2005) 22–30.

[17] F. Fietzke, K. Goedicke, W. Hempel, The deposition of hard crystalline Al_2O_3 layers by means of bipolar pulsed magnetron sputtering, Surface and Coatings Technology 86–87 (1996) 657–663.

[18] S.S. Lin, Effect of fibered morphology on the properties of Al_2O_3 nanoceramic films, Ceramics International 39 (2013) 3157–3163.

[19] W.T. Lim, C.H. Lee, Highly oriented ZnO thin films deposited on Ru/Si substrates, Thin Solid Films 353 (1999) 12–15.

[20] S.S. Lin, The optical properties of Ti-doped TiO_2 nanoceramic films deposited by simultaneous rf and dc magnetron sputtering, Ceramics International 38 (2012) 3129–3134.

[21] G. Laukaitis, S. Lindroos, S. Tamulevičius, M. Leskelä, Stress and morphological development of CdS and ZnS thin films during the SILAR growth on (100) GaAs, Applied Surface Science 185 (2001) 134–139.

[22] T. Schuler, M.A. Aegerter, Optical, electrical and structural properties of sol–gel ZnO:Al coatings, Thin Solid Films 351 (1999) 125–131.

[23] A.F. Carley, P.R. Chalker, J.C. Riviere, M. Wyn Roberts, The identification and characterisation of mixed oxidation states at oxidised titanium surfaces by analysis of X-ray photoelectron spectra, Journal of the Chemical Society, Faraday Transactions 1 (83) (1987) 351–370.

[24] M. Radecka, TiO_2 for photoelectrolytic decomposition of water, Thin Solid Films 451–452 (2004) 98–104.

[25] E.A. Souza, A.O. Santos, R. Landers, F. Cunha, M.A. Macêdo, Structural and electrochemical behavior of tungsten oxide obtained by solid state reaction, Solid State Ionics 177 (2006) 697–701.

[26] Z. Wang, Z. Liu, Z. Yang, S. Shingubara, Characterization of sputtered tungsten nitride film and its application to Cu electroless plating, Micro Engineering 85 (2008) 395–400.

[27] C.D. Wagner, W.M. Riggs, L.E. Davis, J.F. Moulder, G.E. Muilenberg, Handbook of X-ray Photoelectron Spectroscopy, 1979, pp. 68–69, Printed in the United States of America.

[28] Y. Igasaki, H. Saito, The effects of zinc diffusion on the electrical and optical properties of ZnO:Al films prepared by r.f. reactive sputtering, Thin Solid Films 199 (1991) 223–230.

[29] Y. Igasaki, H. Saito, Substrate temperature dependence of electrical properties of ZnO:Al epitaxial films on sapphire, Journal of Applied Physics 69 (1991) 2190–2195.

[30] J.F. Nye, Physical Properties of Crystals: Their Representation by Tensors and Matrices, Oxford Science, New York, 1992.

[31] W. Lukosz, P. Pliska, Determination of thickness, refractive indices, optical anisotropy of, and stresses in SiO_2 films on silicon wafers, Optics Communications 117 (1995) 1–7.

[32] W.F. Smith, J. Hashemi, Foundations of Materials Science and Engineering, fifth Edition, McGraw-Hill, New York233.

[33] D. Liu, B. Zhou, S.H. Yoon, S.B. Kim, H. Ahn, B.C. Prorok, S.H. Kim, D.J. Kim, Determination of the true Young's Modulus of $Pb(Zr_{0.52}Ti_{0.48})O_3$ films by nanoindentation: effects of film orientation and substrate, Journal of the American Ceramic Society 94 (2011) 3698–3701.

[34] R. Saha, W.D. Nix, Effects of the substrate on the determination of thin film mechanical properties by nanoindentation, Acta Materialia 50 (2002) 23–38.

[35] D. Liu, B. Zhou, S.H. Yoon, H.C. Wikle III, Y. Wang, M. Park, B. C. Prorok, D.J. Kim, Effects of the structural layer in MEMS substrates on mechanical and electrical properties of $Pb(Zr_{0.52}Ti_{0.48})O_3$ films, Ceramics International 37 (2011) 2821–2828.

[36] D.C. Van Der Laan, J.W. Ekin, C.C. Clickner, T.C. Stauffer, Delamination strength of YBCO coated conductors under transverse tensile stress, Superconductor Science and Technology 20 (2007) 765–770.

[37] J.L. Hay, G.M. Pharr, Mechanical testing and evaluation, in: H. Kuhn, D. Medlin (Eds.), ASM Handbook, vol. 8, ASM International, Materials Park, OH, 2000, pp. 232–243.

[38] B. Hunsche, M. Vergöhl, H. Neuhäuser, F. Klose, B. Szyszka, T. Matthée, Effect of deposition parameters on optical and mechanical properties of MF- and DC-sputtered Nb_2O_5 films, Thin Solid Films 392 (2001) 184–190.

[39] N. Serpone, D. Lawless, R. Khairutdinov, Subnanosecond relaxation dynamics in TiO_2 colloidal sols (particle sizes $Rp = 1.0$–13.4 nm). Relevance to heterogeneous photocatalysis, Journal of Physical Chemistry 99 (1995) 16655–16661.

[40] D.D. Claudio, A.R. Phani, S. Santucci, Enhanced optical properties of sol–gel derived TiO_2 films using microwave irradiation, Optical Materials 30 (2007) 279–284.

[41] B.E. Sernelius, K.F. Berggren, Z.C. Jin, I. Hamberg, C.G. Granqvist, Band-gap tailoring of ZnO by means of heavy Al doping, Physical Review B 37 (1988) 10244–10248.

[42] E. Mollwo, in: R.G. Breckenridge, B.R. Russell, E.E. Hahn, (Eds.), Proceedings of the Photoconductivity Conference, Wiley, New York, 1954, p. 509.

[43] T. Yamamoto, T. Shiosaki, A. Kawabata, Characterization of ZnO piezoelectric films prepared by rf planar-magnetron sputtering, Journal of Applied Physics 51 (6) (1980) 3113–3120.

[44] B.S. Chiou, S.T. Hsieh, W.F. Wu, Deposition of indium tin oxide films on acrylic substrates by radiofrequency magnetron sputtering, Journal of the American Ceramic Society 77 (7) (1994) 1740–1744.

[45] M.J. Soileau, W.E. Williams, N. Mansour, E.W. Van Stryland, Laser-induced damage and the role of self-focusing, Optical Engineering 28 (1989) 1133–1144.

[46] E.W. Van Stryland, Y.Y. Wu, D.J. Hagan, M.J. Soileau, K. Mansour, Optical limiting with semiconductors, Journal of the Optical Society of America B 5 (1988) 1980–1988.

[47] M.J. Soileau, W.E. Williams, E.W. Van Stryland, Optical power limiter with picosecond response time, IEEE Journal of Quantum Electronics QE 19 (1983) 731–735.

[48] K. Mansour, M.J. Soileau, E.W. Van Stryland, Nonlinear optical properties of carbon-black suspensions (ink), Journal of the Optical Society of America B 3 (1992) 1100–1109.